Online Appendix:
Dynamic Usage Allocation and Pricing for Curb Space Operation

Jisoon Lim and Neda Masoud

Department of Civil and Environmental Engineering,
University of Michigan, Ann Arbor, MI

A Proof of Objective Function Transformation Equivalence

Proposition 1. *The transformed objective function in model (4) is equivalent to the original objective function in model (1) (function (1a)).*

Proof. For any usage $i \in I$ and service periods $(t, t') \in K$,

$$A_i^{(t,t')^2} = (p_i^t + k^{(t,t')}Q_i^{(t,t')})^2 = p_i^{t2} + 2p_i^t k^{(t,t')}Q_i^{(t,t')} + (k^{(t,t')}Q_i^{(t,t')})^2 \text{ and}$$

$$B_i^{(t,t')^2} = (p_i^t - k^{(t,t')}Q_i^{(t,t')})^2 = p_i^{t2} - 2p_i^t k^{(t,t')}Q_i^{(t,t')} + (k^{(t,t')}Q_i^{(t,t')})^2.$$

Then,

$$A_i^{(t,t')^2} - B_i^{(t,t')^2} = 4p_i^t k^{(t,t')}Q_i^{(t,t')} \Longrightarrow \frac{1}{4}\Big[A_i^{(t,t')^2} - B_i^{(t,t')^2}\Big] = p_i^t k^{(t,t')}Q_i^{(t,t')} = p_i^t k^{(t,t')} \cdot \sum_{(j,j')\in J^2} q_{i(j,j')}^{(t,t')}.$$

Therefore, we have proven Proposition 1. □

B Numerical Example of Benders Cuts

We use utility functions introduced in Section 6 to delineate the Benders cuts generation process. Recall the user and outside option utility functions are as follows:

$$f(\tilde{\mathbf{c}}, q_{i,(j,j')}^{(t,t')}) = \Big(F_i^{(t,t')}\gamma_{i,(j,j')}^t(1 - \theta_{\mathrm{pr}i}{}^t\bar{y}_i^t - \theta_{\mathrm{oc}i}{}^t\frac{q_{i,(j,j')}^{(t,t')}}{D_{ij}^{(t,t')}})\Big)q_{i(j,j')}^{(t,t')};$$

$$h(\tilde{\mathbf{c}}, q_{i,(j,0)}^{(t,t')}) = \Big(H_i^t(1 + \frac{\theta_{\mathrm{oc}i}{}^t}{2}\frac{q_{i,(j,0)}^{(t,t')}}{D_{ij}^{(t,t')}})\Big)q_{i(j,0)}^{(t,t')}.$$

Note the Benders decomposition complicating variables vector is fixed in its value ($\tilde{\mathbf{c}} = \tilde{\mathbf{o}} + \{\delta\}$), where the fixed values are indicated by the bar over the variables. Subsequently, gradients of the utility functions with respect to q-variables are as follows:

$$\nabla f(\tilde{\mathbf{c}}, q_{i,(j,j')}^{(t,t')}) = F_i^t\gamma_{i,(j,j')}^t(1 - \theta_{\mathrm{pr}i}{}^t\bar{y}_i^t - \theta_{\mathrm{oc}i}{}^t\frac{q_{i,(j,j')}^{(t,t')}}{D_{ij}^{(t,t')}}) + F_i^t\gamma_{i,(j,j')}^t(-\theta_{\mathrm{oc}i}{}^t\frac{1}{D_{ij}^{(t,t')}})q_{i(j,j')}^{(t,t')}$$

$$= F_i^t \gamma_{i,(j,j')}^t (1 - {\theta_{\text{pr}}}_i^t \bar{y}_i^t) - 2\frac{F_i^t \gamma_{i,(j,j')}^t {\theta_{\text{oc}}}_i^t}{D_{ij}^{(t,t')}} q_{i(j,j')}^{(t,t')};$$

$$\nabla h(\tilde{\mathbf{c}}, q_{i,(j,0)}^{(t,t')}) = H_i^t (1 + \frac{{\theta_{\text{oc}}}_i^t}{2} \frac{q_{i,(j,0)}^{(t,t')}}{D_{ij}^{(t,t')}}) + H_i^t (\frac{{\theta_{\text{oc}}}_i^t}{2} \frac{1}{D_{ij}^{(t,t')}}) q_{i,(j,0)}^{(t,t')}$$

$$= H_i^t + \frac{H_i^t {\theta_{\text{oc}}}_i^t}{D_{ij}^{(t,t')}} q_{i,(j,0)}^{(t,t')}.$$

We may divide each gradient into terms with and without q-variables, and the terms without such variables will be placed on the RHS of the subproblem constraints. Then, the Benders cuts are generated as follows (to prevent notation abusing we have omitted superscript (t, t') and subscript i):

1. The Benders optimality cuts are generated as follows:

$$Q \leq \hat{C}(\tilde{\mathbf{c}}) = \sum_{j' \in J} r_{j'} \hat{\omega}_{\text{2b}j'} + \sum_{j \in J} D_j \hat{\omega}_{\text{2c}j} + \sum_{(j,j') \in J^2} F \gamma_{(j,j')} (1 - \theta_{\text{pr}} y) \hat{\omega}_{\text{3a}(j,j')} + \sum_{j \in J_0} H \hat{\omega}_{\text{3b}j} +$$
$$\sum_{(j,j') \in J_0^2} M_{(j,j')} \delta_{\nu(j,j')} \hat{\omega}_{\text{3d}(j,j')} + \sum_{(j,j') \in J_0^2} M_{(j,j')} \delta_{q(j,j')} \hat{\omega}_{\text{3e}(j,j')},$$

   where $\hat{\omega}$ represent optimal dual variables that correspond to the subproblem constraints indicated in the subscripts.
2. The Benders feasibility cuts are generated as follows:

$$0 \leq \bar{C}(\tilde{\mathbf{c}}) = \sum_{j' \in J} r_{j'} \bar{\omega}_{\text{2b}j'} + \sum_{j \in J} D_j \bar{\omega}_{\text{2c}j} + \sum_{(j,j') \in J^2} F \gamma_{(j,j')} (1 - \theta_{\text{pr}} y) \bar{\omega}_{\text{3a}(j,j')} + \sum_{j \in J_0} H \bar{\omega}_{\text{3c}j} +$$
$$\sum_{(j,j') \in J_0^2} M_{(j,j')} \delta_{\nu(j,j')} \bar{\omega}_{\text{3d}(j,j')} + \sum_{(j,j') \in J_0^2} M_{(j,j')} \delta_{q(j,j')} \bar{\omega}_{\text{3e}(j,j')},$$

   where $\bar{\omega}$ represent unbounded rays of the dual variables (of the subproblem constraints indicated in the subscripts) that prove the subproblem to be infeasible.

Then these two cuts are appended to the master problem as explained in Section 5.3.3.

C Extended Experimental Results

This section includes additional experiments that enhance the insights presented in Section 6. We first show the robustness of the model by introducing a method to handle a more complex form of utility function. Second, we examine the scalability of the model and solution methodologies by exploring a larger number of zones.

C.1 Model robustness: alternative utility function

Our original experiments incorporate linear discount factors concerning the q-variables within the user utility and outside option utility functions. This establishes second-degree polynomial utility functions and warrants KKT optimality conditions outlined in Section 5.1.

The model's ability to accommodate a broader range of diverse utility functions is crucial. It allows to capture a wider array of user traits, strengthening its suitability for practical applications.

In this section, we showcase an alternative form of a user utility function that incorporates a higher-dimensional relationship between the q-variables and discount factors, thereby validating the *robustness* of the model. We retain the optimality condition by providing a piecewise-linear approximation of a utility function.

We specify the alternative user utility function f' as follows:

$$f'(\tilde{\mathbf{o}}, q_{i,(j,j')}^{(t,t')}) = \Big(F_i^t\, \gamma_{i,(j,j')}^t (1 - {\theta_{\text{pr}_i}}^t\, y_i^t - {\theta_{\text{oc}_i}}^t\, (\frac{q_{i,(j,j')}^{(t,t')}}{D_{ij}^{(t,t')}})^2)\Big) q_{i(j,j')}^{(t,t')}.$$

The new utility function has a polynomial sensitivity (of power 2) to an increase in infrastructure utilization. We select this utility function due to its similarity to the BPR function (United States Bureau of Public Roads 1964), which is widely used in evaluating link performance in the presence of congestion. In the BPR function, a vehicle's travel time increases polynomially with road congestion (traffic volume divided by capacity), leading to a reduction in the vehicle's utility. Similarly, in our setup, curb space user utility decreases with the square of infrastructure utilization.

To fully incorporate this alternative utility function into our model, we need to piecewise-linearly approximate the function to ensure linear gradient conditions. More specifically, we need to approximate the q^2 terms included in the first-order derivative of f', which takes the following form:

$$\nabla f'(\tilde{\mathbf{o}}, q_{i,(j,j')}^{(t,t')}) = F_i^t \gamma_{i,(j,j')}^t (1 - {\theta_{\text{pr}_i}}^t y_i^t) - 3\frac{F_i^t \gamma_{i,(j,j')}^t {\theta_{\text{oc}_i}}^t}{{D_{ij}^{(t,t')}}^2} {q_{i(j,j')}^{(t,t')}}^2.$$

Terms ${q_{i(j,j')}^{(t,t')}}^2$ may be approximated into piecewise-linear forms. For our experiments, we divide the domain of q^2 into three intervals of equal lengths for approximation (Note that different piecewise-linear approximations may be utilized, potentially for more adaptable settings. For simplicity, we select to divide the domain into three equal segments.). If the upper bound for q-variables are denoted by $\bar{q}$ – which can be easily substituted into D in our model – the approximation for $i \in I$, $(j, j') \in J^2$, and $(t, t') \in K$ will take the following form:

$${q_{i(j,j')}^{(t,t')}}^2 = \min_{qq,q} \; qq_{i(j,j')}^{(t,t')} \tag{C.1a}$$

$$qq_{i(j,j')}^{(t,t')} \geq \frac{1}{3}\bar{q}_{i(j,j')}^{(t,t')} q_{i(j,j')}^{(t,t')}, \tag{C.1b}$$

$$qq_{i(j,j')}^{(t,t')} \geq \bar{q}_{i(j,j')}^{(t,t')} q_{i(j,j')}^{(t,t')} - \frac{2}{9}{\bar{q}_{i(j,j')}^{(t,t')}}^2, \tag{C.1c}$$

$$qq_{i(j,j')}^{(t,t')} \geq \frac{5}{3}\bar{q}_{i(j,j')}^{(t,t')} q_{i(j,j')}^{(t,t')} - \frac{2}{3}{\bar{q}_{i(j,j')}^{(t,t')}}^2. \tag{C.1d}$$

Objective function (C.1a) sets the qq-variables to approximate the square of q-variables. Constraints (C.1b)-(C.1d) define the three intervals of the approximation as $([0, \frac{1}{3}\bar{q}], [\frac{1}{3}\bar{q}, \frac{2}{3}\bar{q}], [\frac{2}{3}\bar{q}, \bar{q}])$. The minimization of function (C.1a) is effective as the square function is convex. When constraints (C.1b)-(C.1d) are appended to the model and replace q^2 terms with qq terms, the minimization is conserved as ∇f is maximized when qq is minimized. For the Benders decomposition algorithm, the additional constraints are added to the subproblem(s), and Benders cuts are generated from the subsequent dual subproblems.

To evaluate the performance of the BIVIC algorithm under the new user utility function, we conduct additional experiments for the three-zone scenario. The new experiments mimic an

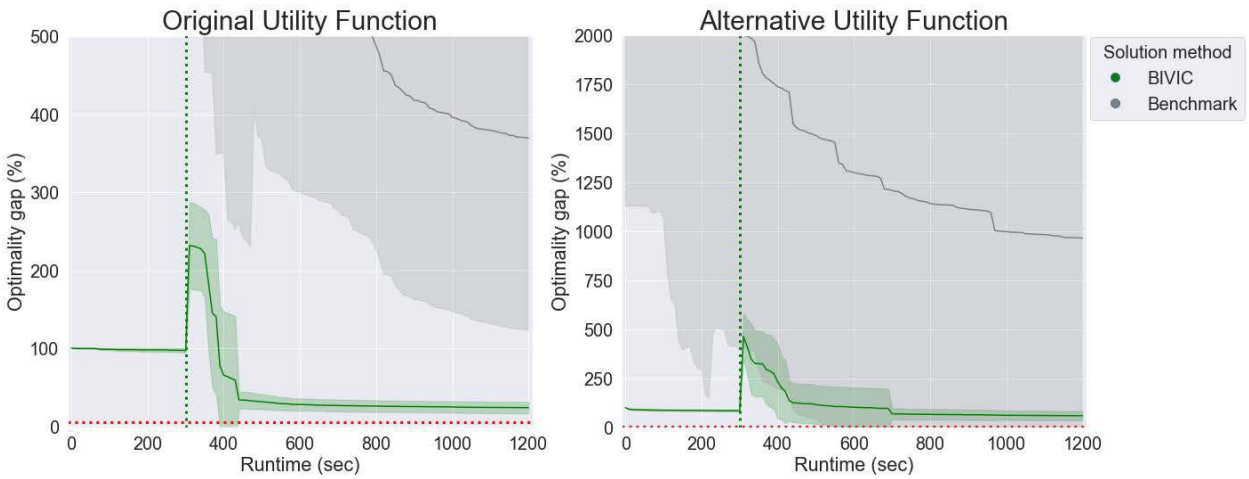

Figure C.1: Average optimality gaps for the BIVIC and benchmark methods under the original utility function (left subfigure) and the alternative utility function (right subfigure) for the three-zone scenario. The green and grey lines show the average optimality gap of the BIVIC algorithm and the benchmark, respectively as a percentage. The shaded regions show the plus/minus of one standard deviation over the ten randomly generated experiments. A red dotted horizontal line indicates the 5% optimality gap threshold. A green dotted vertical line indicates the time of the switch from the first phase to the second phase of the BIVIC algorithm.

experimental setup delineated in Section 6.2. We test 10 randomly generated instances to show the average performance using the BIVIC algorithm and the benchmark branch-and-cut method.

Figure C.1 compares the average optimality gaps obtained by the BIVIC solution algorithm and the benchmark, under the linear utility function and the second-degree polynomial utility function. Figure C.2 provides a similar comparison for the upper and lower solution bounds. The figures' layouts are similar to those of Figures 3-4.

The investigation shows that using a higher-degree polynomial utility function significantly complicates the benchmark (note the y-axis scales in the corresponding subfigures are quadrupled). Nevertheless, the BIVIC algorithm reports more consistent computation results over different forms of the utility function. The findings highlight the mathematical model's adaptability to intricate user traits and the solution algorithm's ability to deliver consistent performance.

C.2 Model scalability: extended number of zones

As noted in our problem description, we implement curb space zones in our model, grouping individual curb spaces according to factors such as proximity, user comfort, enforcement strategy, etc. There is no constraint on how many spaces each zone can encompass, offering potential for real-world applications with a limited number of zones. Yet, assessing the *scalability* of the model remains vital. Therefore, we explore larger scenarios with additional numbers of zones to evaluate the efficiency of our solution algorithms. As discussed in Section 6.2, the complexity of the mathematical model increases the most with the addition of zones compared to the number of usages or time epochs.

Experimental results in this section consider three- to six-zone scenarios. For each scenario, 10 experiments are conducted with randomly sampled values for price and occupancy sensitivities, both within the range $[0, 1.5]$. For each experiment, computations are terminated at a 5% optimality gap or after a preset total runtime, whichever comes first.

We use the BIVIC algorithm for computation, which is shown to be most effective in reporting

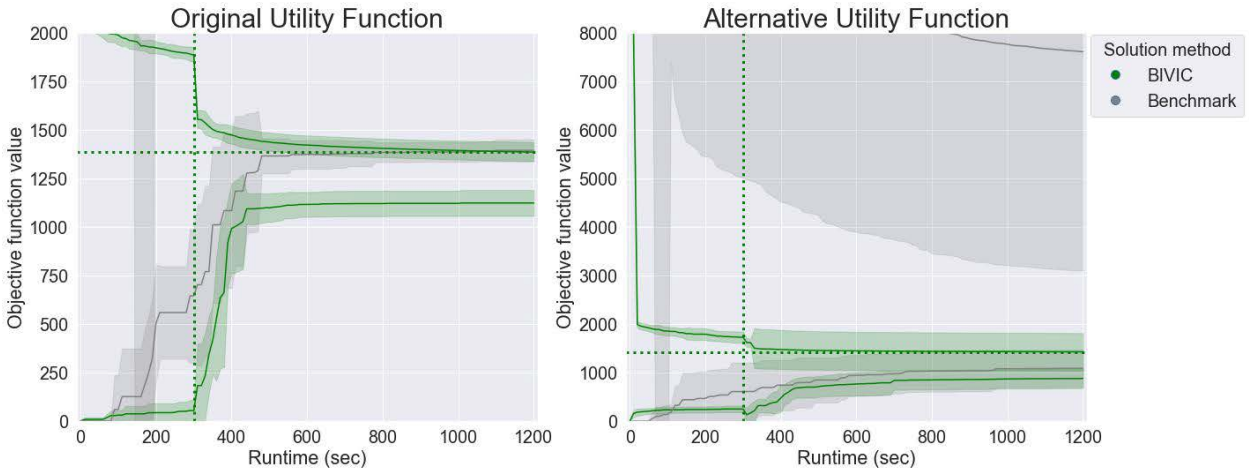

Figure C.2: Upper and lower solution bounds for the BIVIC and benchmark methods under the original utility function (left subfigure) and the alternative utility function (right subfigure) for the three-zone scenario. The upper/lower green and grey lines show the upper/lower bounds of the solutions for the BIVIC algorithm and the benchmark, respectively. The shaded regions show the plus/minus of one standard deviation over the ten randomly generated experiments. A green dotted vertical line indicates the time of the switch from the first phase to the second phase of the BIVIC algorithm. A green dotted horizontal line indicates the average optimal objective function value of the experiments.

# zones	Phase switch time (min)	Total algorithm runtime (min)
Three	5	20
Four	10	60
Five	15	120
Six	30	180

Table C.1: Phase switch time and total algorithm runtime (in minutes).

quality results. Given the larger scales of the new study horizons, we extend the computation time. The phase switch time and total algorithm runtime are outlined in Table C.1.

Figure C.3 depicts the experimental results. The left and right subfigures show the average optimality gaps and upper and lower solution bounds over the ten experiments for three- to six-zone scenarios (represented by different colors), respectively. The shaded regions show the plus/minus of one standard deviation over the experiments.

We observe that the BIVIC algorithm is capable of identifying a quality solution within the preset algorithm runtime. Thus, we conclude that the algorithm reliably converges when given adequate runtime.

D Parameters for Numerical Experiments

This section includes details of parameter values used for numerical experiments presented in Section 6.

Demand Table D.1 expresses single-, two-, and three-zone scenarios' demands tuples ($D_{ij}^{(t,t')}$) of usage $i \in I$ at zone $j \in J$ for time epoch $t \in T$, in the number of spaces. Demand tuples at each time epoch are further distinguished for users requiring service periods (t, t'), where the three items

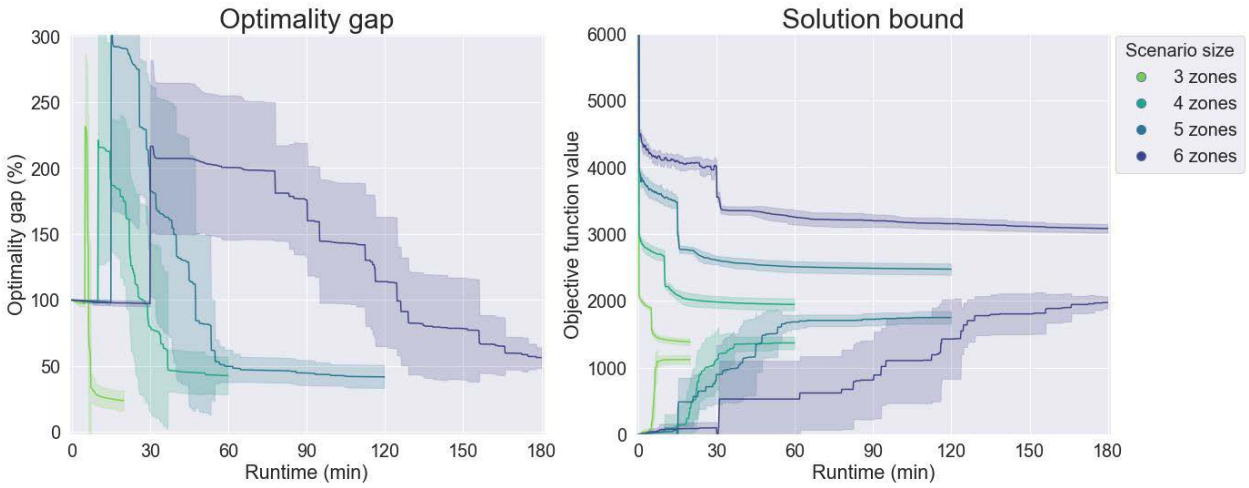

Figure C.3: Average optimality gap (left subfigure) and upper and lower solution bounds (right subfigure) for three- to six-zone scenarios. The lines in different colors denote the results (optimality gaps and bounds) for the corresponding problem size. The shaded regions show the plus/minus of one standard deviation over the ten randomly generated experiments.

in a tuple indicate users that have service periods with $t' = t$ (a user occupies a space for one period), $t' = t + 1$ (two periods), and $t' = t + 2$ (three periods), in order.

Service zone discount factor For the two- and three-zone scenarios, Table D.2 and D.3 respectively express tuples of service zone discount factors ($\gamma^t_{i(j,j')}$) between original zone $j \in J$ and service (actual) zone $j' \in J$ at time $t \in T$. The tuples indicate discount factors for usages ($i \in I$) PARK, PUDO, LUL, and MIC, in order. For the single-zone scenario, $\gamma^t_{i(j,j')} = 1 \ \forall i \in I, (j, j') \in J^2, t \in T$.

User and outside option base utilities Table D.4 expresses user (F^t_i) and outside option (H^t_i) base utilities for usage $i \in I$ at time $t \in t$ for the single-, two-, and three-zone scenarios.

E Heatmaps for User Occupancy Response Analysis

Section 6.3 uses various heatmaps (Figures E.1-E.7) to report occupancy response analysis. Dimensions of the heatmap figures are large, so we present those figures in this section for presentation purposes.

References

United States Bureau of Public Roads (1964). *Traffic assignment manual for application with a large, high speed computer*. U. S. Dept. of Commerce, Bureau of Public Roads, Office of Planning, Urban Planning Division.

			Usage (i)				Total
			PARK	PUDO	LUL	MIC	
Single-zone	j = Zone 1	$t=1$	(2.56/1.82/0.85)	(0.98/0.61/0.34)	(2.45/1.62/0.83)	(1.66/0.91/0.52)	15.15
		$t=2$	(2.82/2.01/0.99)	(2.59/1.50/0.72)	(3.79/2.30/1.31)	(2.02/1.35/0.72)	22.12
		$t=3$	(0.93/0.65/0.35)	(1.08/0.66/0.34)	(1.31/0.93/0.48)	(1.80/1.46/0.66)	10.65
		$t=4$	(2.65/1.32/-)	(0.55/0.33/-)	(2.09/1.05/-)	(1.11/0.68/-)	9.77
		$t=5$	(4.45/-/-)	(4.83/-/-)	(0.82/-/-)	(2.08/-/-)	12.19
Two-zone	j = Zone 1	$t=1$	(1.92/1.29/0.72)	(1.46/1.05/0.49)	(2.21/1.87/0.96)	(2.10/1.51/0.67)	16.26
		$t=2$	(1.42/0.98/0.41)	(2.15/1.73/0.93)	(1.29/1.04/0.53)	(1.51/0.99/0.57)	13.57
		$t=3$	(2.31/1.82/0.82)	(1.40/0.97/0.50)	(0.91/0.74/0.32)	(1.05/0.73/0.36)	13.56
		$t=4$	(2.13/1.07/-)	(3.62/1.66/-)	(1.29/0.58/-)	(2.03/1.05/-)	13.91
		$t=5$	(4.50/-/-)	(3.96/-/-)	(1.76/-/-)	(2.86/-/-)	11.94
	j = Zone 2	$t=1$	(1.57/0.92/0.51)	(1.89/1.17/0.75)	(1.56/1.00/0.52)	(1.94/1.15/0.60)	11.85
		$t=2$	(1.36/0.87/0.52)	(2.05/1.27/0.67)	(1.63/1.08/0.51)	(1.69/1.49/0.74)	13.44
		$t=3$	(1.50/0.91/0.52)	(1.00/0.70/0.31)	(1.62/1.01/0.46)	(1.93/1.19/0.70)	11.82
		$t=4$	(1.94/0.98/-)	(1.27/0.74/-)	(2.14/1.05/-)	(2.45/1.25/-)	13.09
		$t=5$	(3.21/-/-)	(2.10/-/-)	(1.13/-/-)	(3.35/-/-)	9.79
Three-zone	j = Zone 1	$t=1$	(0.94/0.75/0.32)	(1.07/0.65/0.35)	(1.59/1.05/0.46)	(2.09/1.23/0.66)	11.15
		$t=2$	(0.98/0.76/0.35)	(1.65/0.98/0.46)	(1.16/0.67/0.30)	(1.25/1.02/0.49)	10.07
		$t=3$	(1.38/1.07/0.53)	(1.98/1.34/0.61)	(0.98/0.68/0.30)	(2.06/1.32/0.69)	12.93
		$t=4$	(1.34/0.68/-)	(3.09/1.54/-)	(1.22/0.66/-)	(1.86/1.13/-)	11.51
		$t=5$	(2.87/-/-)	(4.20/-/-)	(1.89/-/-)	(3.42/-/-)	12.38
	j = Zone 2	$t=1$	(3.84/3.00/1.40)	(4.12/2.62/1.33)	(3.39/2.35/0.98)	(2.16/1.39/0.75)	27.32
		$t=2$	(3.93/2.40/1.46)	(3.30/1.99/0.96)	(3.08/1.95/1.05)	(4.40/2.52/1.31)	28.34
		$t=3$	(4.28/3.57/1.48)	(2.47/2.04/1.10)	(2.80/2.10/1.08)	(2.86/2.01/1.07)	26.84
		$t=4$	(5.88/2.36/-)	(6.77/3.40/-)	(4.64/2.07/-)	(4.15/1.93/-)	31.20
		$t=5$	(9.72/-/-)	(6.38/-/-)	(7.20/-/-)	(5.56/-/-)	28.86
	j = Zone 3	$t=1$	(1.57/0.96/0.41)	(2.02/1.42/0.59)	(1.41/1.11/0.45)	(2.15/1.32/0.74)	14.16
		$t=2$	(1.51/1.15/0.47)	(1.91/1.33/0.60)	(1.49/0.89/0.50)	(2.37/1.29/0.69)	14.20
		$t=3$	(1.39/0.99/0.54)	(1.04/0.77/0.32)	(1.44/0.96/0.47)	(1.73/1.28/0.73)	11.66
		$t=4$	(2.16/1.03/-)	(1.21/0.62/-)	(1.85/0.97/-)	(2.72/1.29/-)	11.84
		$t=5$	(2.57/-/-)	(2.12/-/-)	(1.01/-/-)	(4.06/-/-)	9.76

Table D.1: Demand matrix for single-, two-, and three-zone scenarios.

Original zone \ Service zone	$j'=1$	$j'=2$
$j=1$	(1.0/1.0/1.0/1.0)	(0.6/0.3/0.0/0.5)
$j=2$	(0.9/0.6/0.0/0.5)	(1.0/1.0/1.0/1.0)

Table D.2: Service zone discount factor matrix (for usages PARK/PUDO/LUL/MIC) for the two-zone scenario.

Original zone \ Service zone	$j'=1$	$j'=2$	$j'=3$
$j=1$	(1.0/1.0/1.0/1.0)	(0.7/0.6/0.0/0.5)	(0.5/0.3/0.0/0.2)
$j=2$	(0.7/0.6/0.0/0.5)	(1.0/1.0/1.0/1.0)	(0.5/0.3/0.0/0.2)
$j=3$	(0.7/0.5/0.0/0.3)	(0.7/0.5/0.0/0.3)	(1.0/1.0/1.0/1.0)

Table D.3: Service zone discount factor matrix (for usages PARK/PUDO/LUL/MIC) for the three-zone scenario.

		Single-zone scenario				Two-zone scenario				Three-zone scenario			
F_i^t		Usage (i)				Usage (i)				Usage (i)			
		PARK	PUDO	LUL	MIC	PARK	PUDO	LUL	MIC	PARK	PUDO	LUL	MIC
Time (t)	1	3.0	2.0	3.0	2.0	5.0	6.0	5.0	4.0	5.0	6.0	5.0	4.0
	2	6.0	5.0	4.0	4.0	5.0	6.0	5.0	4.0	5.0	6.0	5.0	4.0
	3	6.0	6.0	4.0	3.0	8.0	6.0	5.0	4.0	8.0	6.0	5.0	4.0
	4	5.0	4.0	1.0	2.0	8.0	7.0	5.0	5.0	8.0	7.0	5.0	5.0
	5	4.0	5.0	2.0	2.0	7.0	7.0	5.0	6.0	7.0	7.0	5.0	6.0
H_i^t		PARK	PUDO	LUL	MIC	PARK	PUDO	LUL	MIC	PARK	PUDO	LUL	MIC
Time (t)	1	1.00	0.66	0.42	0.66	1.25	1.50	0.50	1.00	1.25	1.50	0.50	1.00
	2	1.66	1.66	0.57	1.00	1.25	1.50	0.50	0.80	1.25	1.50	0.50	0.80
	3	1.66	2.00	0.57	0.75	2.00	1.20	0.50	0.80	2.00	1.20	0.50	0.80
	4	1.66	1.33	0.14	0.50	2.00	1.40	0.50	1.00	2.00	1.40	0.50	1.00
	5	1.33	1.66	0.28	0.50	1.75	1.40	0.50	1.20	1.75	1.40	0.50	1.20

Table D.4: User and outside option base utility matrices for the single-, two-, and three-zone scenarios.

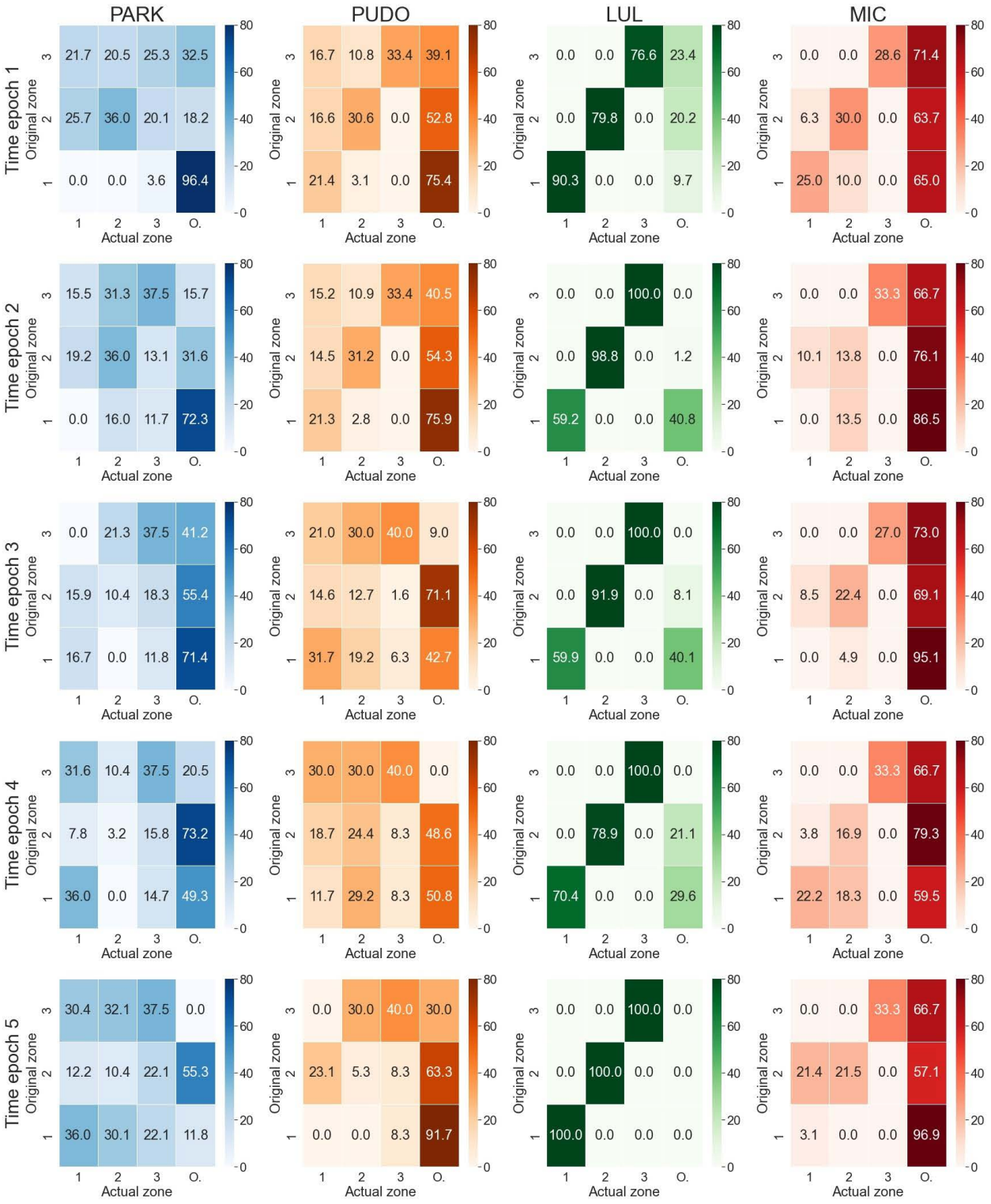

Figure E.1: User occupancy percentage for scenario (1.0,1.0). The rows and columns of each heatmap indicate the original zone (j) and the service (actual) zone (j'), respectively, i.e., (j, j'), $j \in J, j' \in J_0$. The rightmost column of each heatmap indicates the proportion of users who forfeit curb space participation and use an outside option.

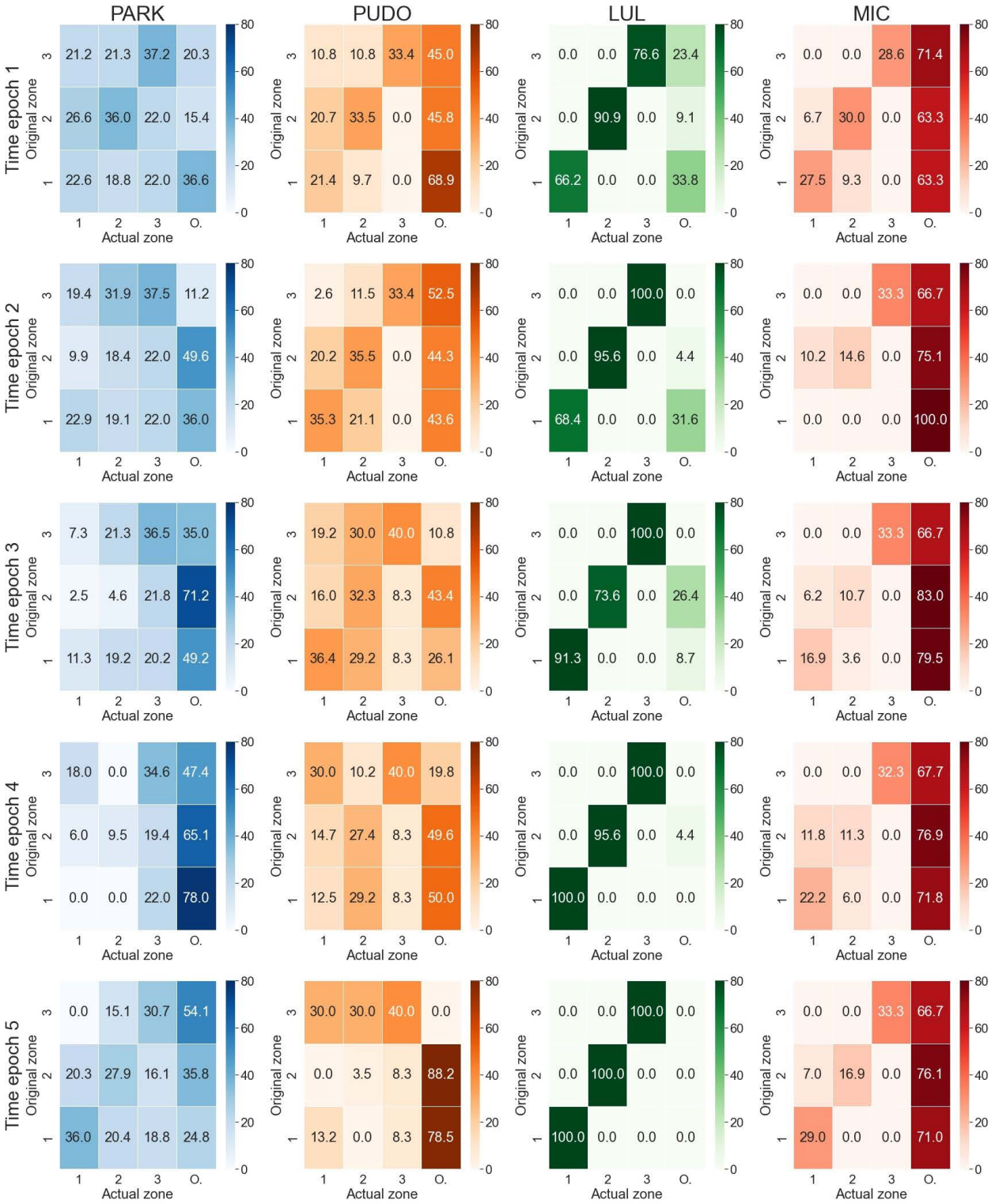

Figure E.2: User occupancy percentage for scenario (0.0,1.0). The rows and columns of each heatmap indicate the original zone (j) and the service (actual) zone (j'), respectively, i.e., (j, j'), $j \in J, j' \in J_0$. The rightmost column of each heatmap indicates the proportion of users who forfeit curb space participation and use an outside option.

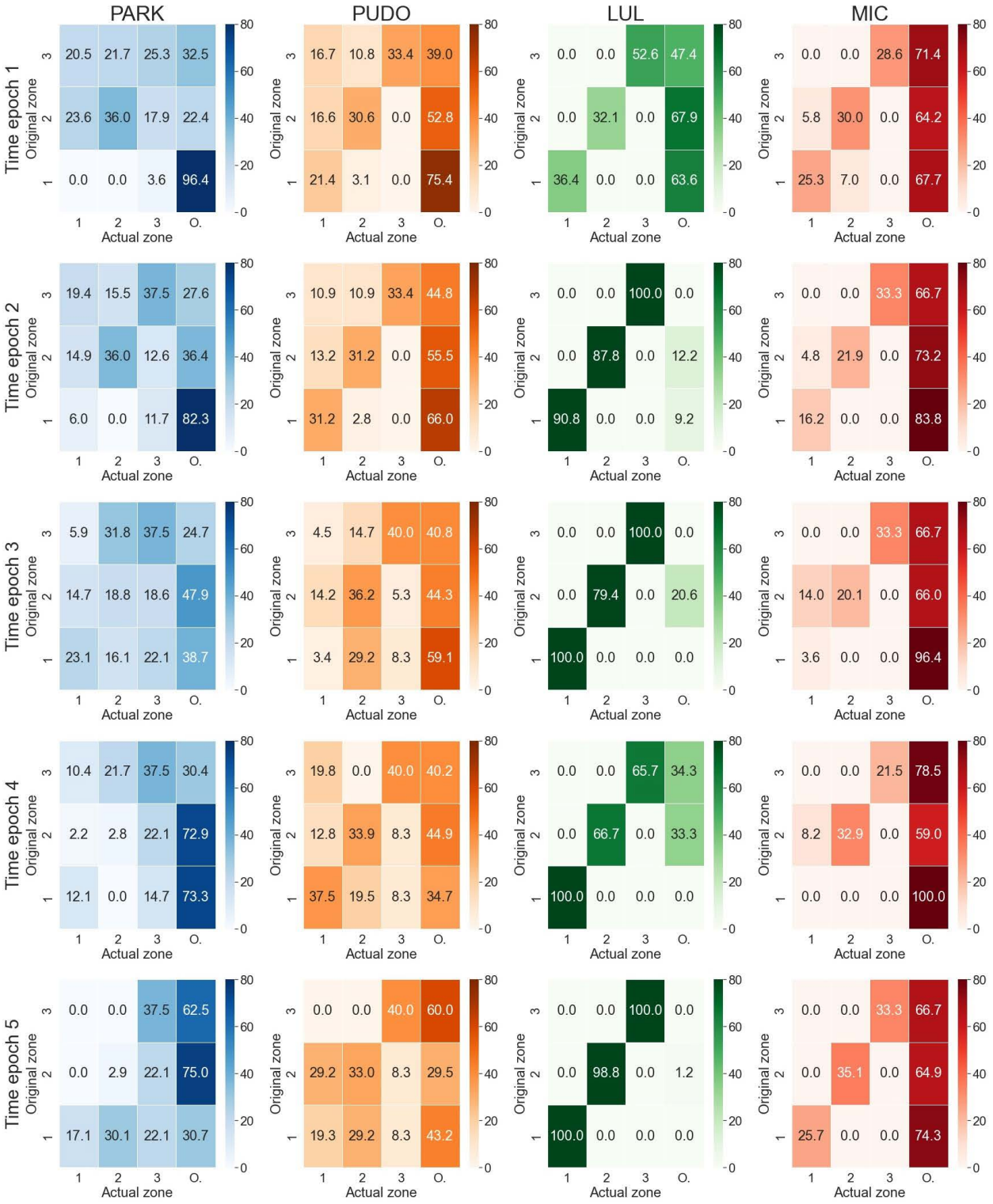

Figure E.3: User occupancy percentage for scenario (2.0,1.0). The rows and columns of each heatmap indicate the original zone (j) and the service (actual) zone (j'), respectively, i.e., (j, j'), $j \in J, j' \in J_0$. The rightmost column of each heatmap indicates the proportion of users who forfeit curb space participation and use an outside option.

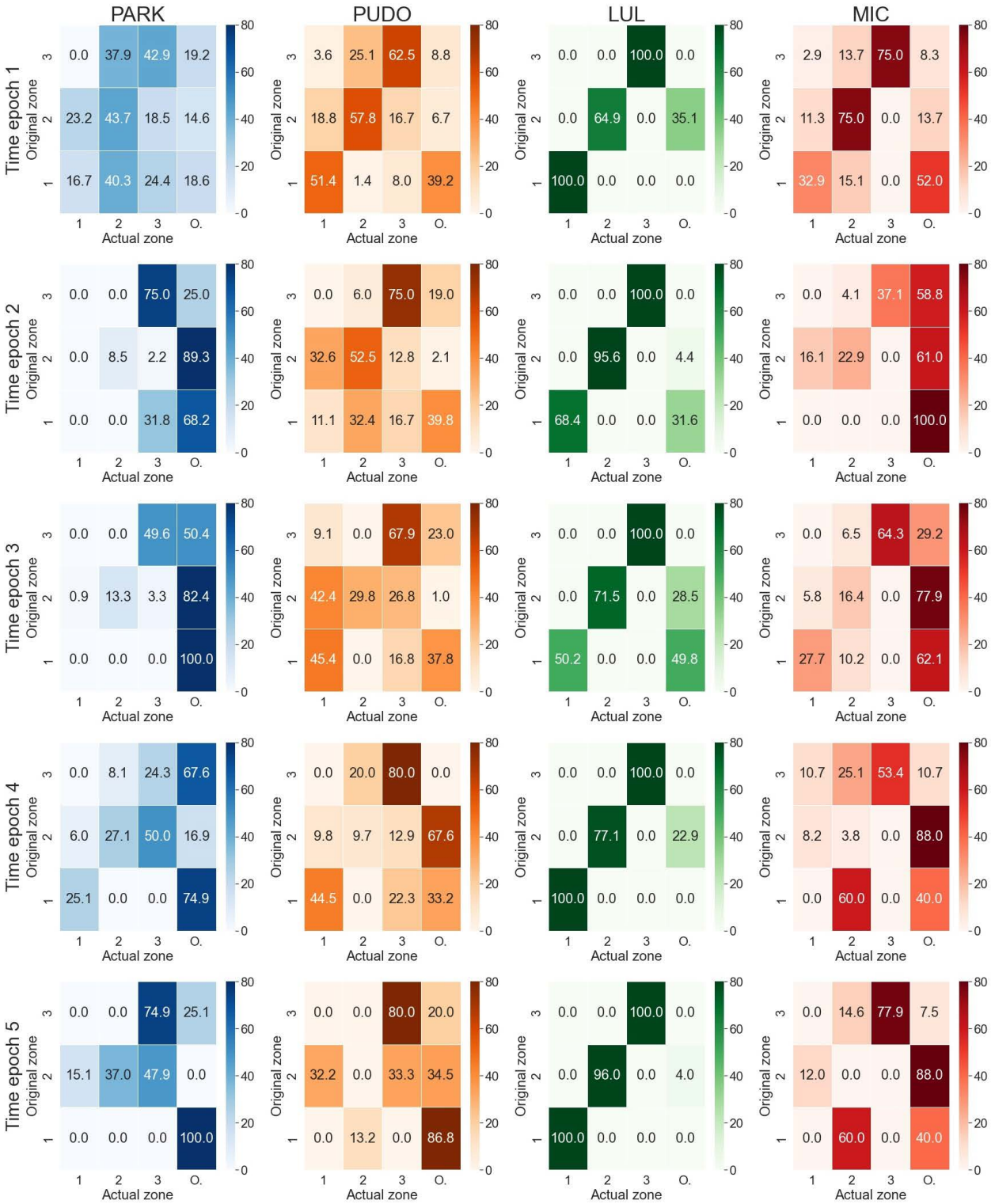

Figure E.4: User occupancy percentage for scenario (1.0,0.5). The rows and columns of each heatmap indicate the original zone (j) and the service (actual) zone (j'), respectively, i.e., (j, j'), $j \in J, j' \in J_0$. The rightmost column of each heatmap indicates the proportion of users who forfeit curb space participation and use an outside option.

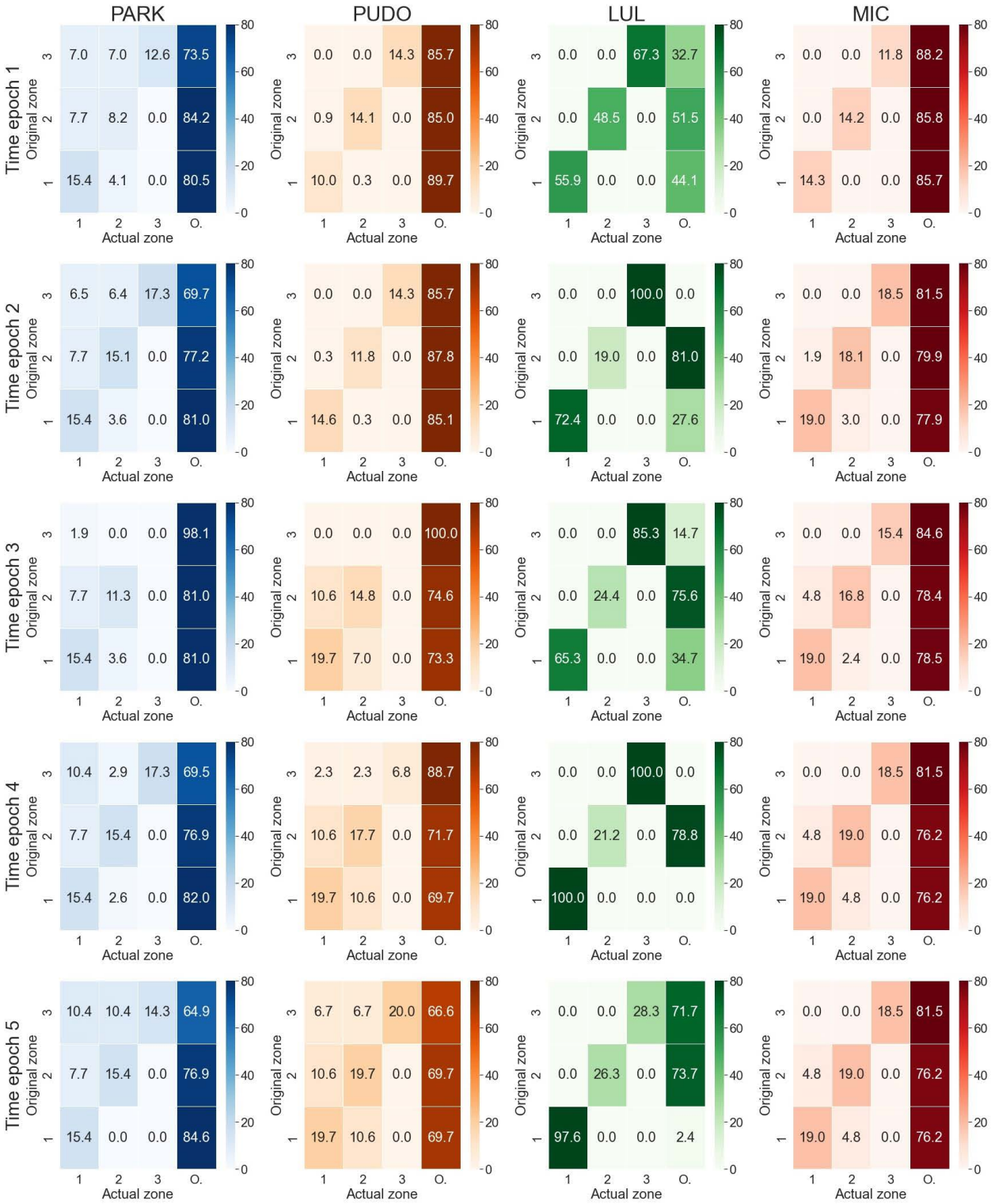

Figure E.5: User occupancy percentage for scenario (1.0,1.5). The rows and columns of each heatmap indicate the original zone (j) and the service (actual) zone (j'), respectively, i.e., (j, j'), $j \in J, j' \in J_0$. The rightmost column of each heatmap indicates the proportion of users who forfeit curb space participation and use an outside option.

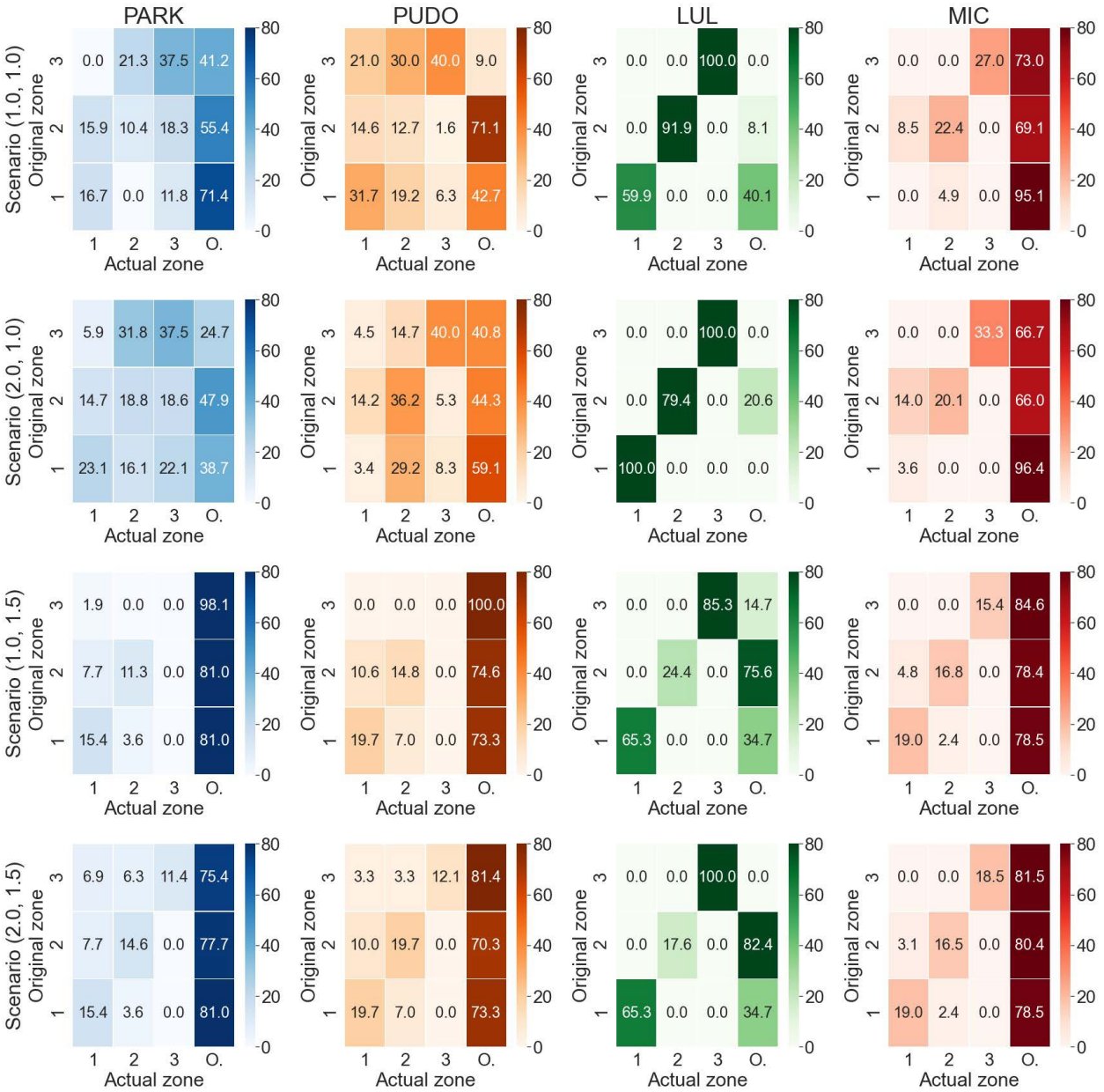

Figure E.6: User occupancy percentage at time epoch 3 for the selected scenarios. The rows and columns of each heatmap indicate the original zone (j) and the service (actual) zone (j'), respectively, i.e., (j, j'), $j \in J, j' \in J_0$. The rightmost column of each heatmap indicates the proportion of users who forfeit curb space participation and use an outside option.

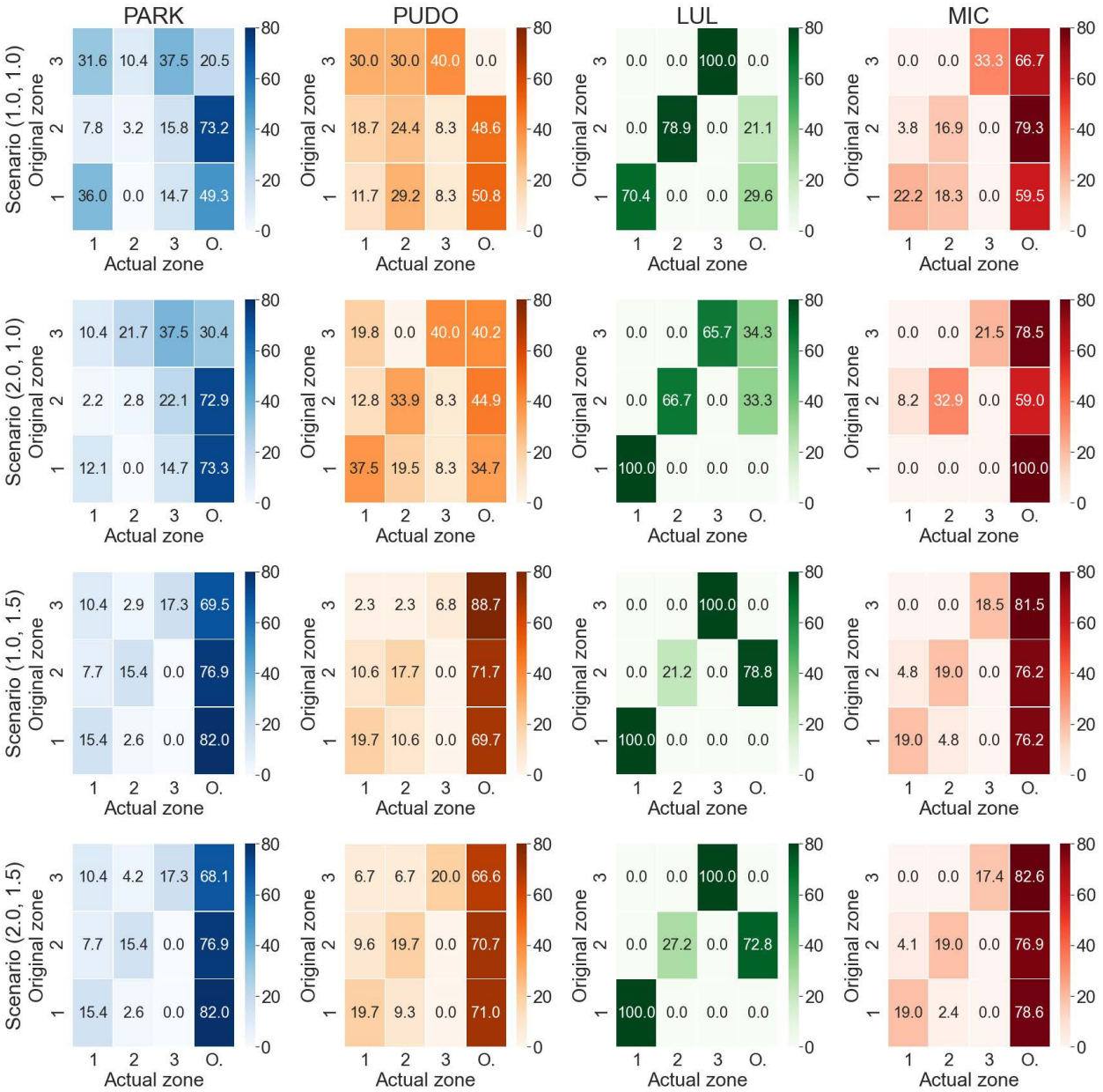

Figure E.7: User occupancy percentage at time epoch 4 for the selected scenarios. The rows and columns of each heatmap indicate the original zone (j) and the service (actual) zone (j'), respectively, i.e., (j, j'), $j \in J, j' \in J_0$. The rightmost column of each heatmap indicates the proportion of users who forfeit curb space participation and use an outside option.